Energy & Environmental Science

Cite this: *Energy Environ. Sci.*, 2012, **5**, 7878

www.rsc.org/ees

COMMUNICATION

# Highly stable Si-based multicomponent anodes for practical use in lithium-ion batteries†

**Jung-In Lee, Nam-Soon Choi and Soojin Park***

***Received 14th February 2012, Accepted 3rd May 2012***
**DOI: 10.1039/c2ee21380j**

**We demonstrate a simple process to synthesize silicon-based multicomponents *via* a high-temperature annealing of bulk silicon monoxide in the presence of sodium hydroxide. The carbon-coated Si-based anodes exhibit a highly stable cycling performance (capacity retention of 99.5% after 200 cycles) with a reversible charge capacity of 1280 mA h $g^{-1}$.**

Lithium-ion batteries (LIBs) are widely regarded as suitable power sources for mobile electronic products, power tools, and upcoming electric vehicles (EVs). The rapid development of electronic devices and EVs requires a much higher energy and power density for anodes, compared to those of conventional carbon-based materials (*e.g.*, natural graphite, MCMB (mesocarbon microbeads)).[1–3] Therefore, pure elements (*e.g.*, Si, Ge, Al, Sn, Sb, *etc.*), their alloys, and metal oxides (*e.g.*, $Fe_2O_3$, NiO, CuO, *etc.*) have been explored as promising electrodes in LIBs.[4–9] Among them, Si-based materials have been attracting much attention, as they offer the essential advantages of abundant sources and a high theoretical capacity. However, the practical use of these materials has been frustrated by rapid capacity fading, due to the unavoidable large volume changes during charging and discharging.[10]

The use of nanostructured Si-based electrodes, including nanoparticles, nanowires, nanotubes, and nanoporous structures, provides an effective solution to achieve a high reversible capacity, an improved rate capability, and a stable cycle performance, because the nanomaterials have enhanced active sites due to a high surface area and favor the electronic and ionic diffusion.[4,11,12] However, some intrinsic drawbacks, including high-cost, low packing density (*i.e.*, low volumetric energy density), and a serious surface side-reaction due to the high surface area, remain to be solved to maximize the advantages of the nanostructured electrodes.

Nanostructuring of microscale electrode materials can be one of the best solutions to increase the volumetric energy density. The examples are nanoscale active materials uniformly confined to a microscale matrix,[13–15] microscale active materials within a nanostructured conductive network,[16,17] and microscale active material with an nanostructured coating layer.[18,19]

Among them, a silicon monoxide (SiO) based composite electrode is one of the good candidates which can exhibit highly stable cycling retention in LIBs.[20–23] SiO shows better cycling performance than silicon composite electrodes. The first lithiation process results in the formation of nano-sized amorphous Si clusters surrounded by lithium oxide and lithium silicate that act as buffer layers to minimize the volume changes during the charging and discharging. The combination of nano-sized active material and micro-scale inactive

*Interdisciplinary School of Green Energy, Ulsan National Institute of Science and Technology, Ulsan, Korea 689-798. E-mail: spark@unist.ac.kr; Fax: +82-52-217-2909*

† Electronic supplementary information (ESI) available: XRD patterns of Si-based multicomponents and cycling performance of c-Si-multi-electrodes. See DOI: 10.1039/c2ee21380j

## Broader context

The rapid development of electronic devices and electric vehicles requires a much higher energy and power density for anodes, compared to those of conventional carbon-based materials. Therefore, Si-based materials have been attracting much attention, as they offer the essential advantages of abundant sources and a high theoretical capacity. However, these materials have not been used in the practical lithium-ion batteries, due to the unavoidable large volume changes during charging and discharging. Nanostructuring of Si-based electrodes provides an effective solution to the electrochemical properties, including a high reversible capacity and a stable cycle performance. However, some intrinsic drawbacks, like high-cost, low volumetric energy density and a serious side reaction, should be solved. Chemical processing of commercially available micro-scale silicon monoxide is one of the good solutions to solve several problems of nanostructured Si-based materials. In this study, we demonstrate a simple method for preparing Si–SiO–$SiO_2$ multicomponents from commercially available solid SiO particles *via* high-temperature annealing in the presence of sodium hydroxide. Combining a high reversible capacity of Si with a stable cycle performance of SiO enabled us to make high-performance anode materials in lithium-ion batteries. The carbon-coated Si-based electrodes showed a high reversible capacity of 1280 mA h $g^{-1}$ and an excellent cycle retention of 99.5% at 0.2 C after 200 cycles.

materials provides a significantly improved cycling performance. However, SiO-based composite electrodes exhibit a poor initial coulombic efficiency, due to a conversion reaction.

Herein, we present a simple route for synthesizing Si–SiO–$SiO_2$ three-component particles, consisting of a Si/SiO core and a crystalline $SiO_2$ shell, from commercially available SiO bulk particles *via* a thermal annealing process in the presence of sodium hydroxide (NaOH). The Si and SiO act as active materials in LIBs, while the crystalline $SiO_2$ serves as a buffer material. The combination of high specific capacity of Si and highly stable cycling performance of SiO exhibits high-performance electrochemical properties, including a high reversible capacity of 1280 mA h $g^{-1}$ and an excellent cycle retention of 99.5% at 0.2 C after 200 cycles, compared to that at 0.1 C rate.

Despite a variety of physical and chemical investigations of amorphous SiO, there is still no unambiguous structural model.[24–26] Recently, a plausible model has been proposed, in which both clusters of amorphous Si and amorphous $SiO_2$ are surrounded by a suboxide matrix.[27] Owing to the microstructures of solid SiO, it is thermodynamically unstable at all temperatures. When SiO was thermally annealed at high temperatures (>900 °C) for several hours, it decomposes to Si and $SiO_2$.[22,28] In cases of commercially available solid SiO particles, the decomposition of SiO was not observed at <900 °C.

We used commercially available amorphous SiO (325 mesh) particles to synthesize Si-based multicomponents, consisting of Si, SiO, and $SiO_2$, using thermal decomposition of SiO in the presence of NaOH (scheme of Fig. 1a). When a mixture of bulk SiO powders (10 g) and NaOH (0.5 g) was thermally annealed at 800 °C for a short period of time (10 min), the decomposition of the SiO was clearly observed (Fig. 1). We propose the chemical reaction between SiO and NaOH occurring on the surface of particles as follows: $3SiO + 2NaOH \rightarrow Na_2SiO_3 + H_2 + Si + SiO_2$.

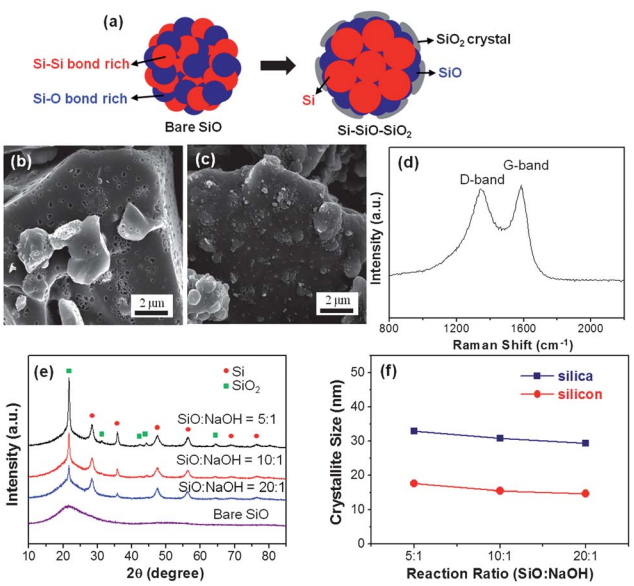


**Fig. 1** Synthesis of an Si-based multicomponent from bulk SiO particles *via* thermal annealing in the presence of NaOH. (a) Schematic illustration for the conversion of bare SiO to Si–SiO–$SiO_2$ three-components, (b) SEM image of Si-based multicomponents, SEM image (c) and Raman spectrum (d) of carbon-coated Si-based multicomponents, (e) XRD patterns of Si-based multicomponents as a function of NaOH amount, and (f) calculation of silica and silicon crystallite size as a function of NaOH amount.

During the thermal annealing of the SiO in the presence of NaOH, sodium silicate ($Na_2SiO_3$) formed on the surface of the particles (ESI, Fig. S1†), and the evolution of $H_2$ gas produced several pores on the particle surfaces, as shown in the scanning electron microscopy (SEM) image (Fig. 1b). The formed $Na_2SiO_3$ was completely removed by rinsing with 10% acetic acid. Subsequently, the carbon coating process was carried out on the surface of the Si-based multicomponents by thermal decomposition of acetylene gas at 900 °C for 10 min (Fig. 1c). The quality of the carbon layers was investigated by Raman scattering. It confirmed that two peaks at ~1360 and ~1580 $cm^{-1}$ corresponding to the disordered (D) and the graphene (G) bands were shown, respectively, indicating the formation of amorphous carbon with an $I_D/I_G$ ratio of 2.2 (Fig. 1d).

In order to investigate the effect of the NaOH amount on the thermal decomposition of SiO particles, the weight ratios of SiO to NaOH were spanned from 20 : 1 to 5 : 1 under a fixed annealing condition (800 °C for 10 min). The X-ray diffraction (XRD) analysis indicated that crystalline Si, crystalline $SiO_2$ (cristobalite), and amorphous $SiO_x$ phases were formed. As the amount of NaOH increased, a peak intensity of the cristobalite was significantly increased, indicating the thermal decomposition of a large portion of the SiO (Fig. 1e). The amounts of Si, $SiO_x$, and crystalline silica may not be calculated quantitatively from the peak intensities of XRD patterns. However, the relative amount of Si and crystalline silica can be estimated from samples obtained at different weight ratios of SiO and NaOH as shown in Fig. 1e.

From the XRD results, we calculated the crystallite size of the Si and the cristobalite as a function of the NaOH amount, using the Scherrer equation, $L = 0.9\lambda/(B \cdot \cos\theta)$, where $L$ is the diameter of the crystallites, $\lambda$ is the X-ray wavelength, $B$ is the full width at half-maximum, and $\theta$ is the Bragg angle.[29] Both the Si and the $SiO_2$ crystallite sizes increased with an increasing amount of NaOH (Fig. 1f). In addition, the control of annealing time at a fixed temperature tuned the amount of Si, $SiO_x$, and cristobalite (ESI, Fig. S2†).

When a solid SiO powder was thermally annealed at >900 °C for several hours, the thermal disproportionation of SiO occurred, in which nanocrystalline Si was dispersed within an amorphous $SiO_2$ matrix. In contrast, thermal annealing of SiO in the presence of NaOH induced the decomposition of SiO at a lower temperature for a short period of time. We propose the conversion of the SiO to the Si-based multicomponents during the thermal annealing process, as follows: (i) the hydrothermal reaction or high temperature annealing of amorphous $SiO_2$ in the presence of NaOH led to the formation of crystalline $SiO_2$.[30,31] Amorphous $SiO_2$ was thermally annealed in the presence of NaOH (weight ratio of SiO to NaOH = 20 : 1) at the same condition as those used in the SiO. A great part of amorphous silica was converted into crystalline silica (cristobalite) (ESI, Fig. S3†). The amorphous SiO also has the amorphous $SiO_2$ in the outermost shell. The amorphous $SiO_2$ in the outer shell reacts with NaOH to make cristobalite at high temperature (ESI, Fig. S4†). It was confirmed by time-of-flight secondary ion mass spectrometry analysis (ESI, Fig. S5†). (ii) Simultaneously, amorphous SiO was decomposed to nanocrystalline Si and amorphous $SiO_x$ matrix. As the annealing time increased, the amorphous $SiO_x$ in the matrix was continuously converted into crystalline silica, so that the thickness of crystalline

silica increased. Whereas, in the inner regions, the annealing process induced the transport of oxygen from Si–O bond rich regions inside SiO particles, resulting in the increase of Si–Si bond rich regions (that is, an increase of Si crystallite size) inside the SiO particles. (iii) The resulting particles, Si-based multicomponents (Si–SiO–$SiO_2$ three-component), were composed of an Si/SiO core and a cristobalite shell. And (iv) the relative amount of NaOH to SiO and annealing time affect the contents of the resulting crystalline Si and cristobalite.

We investigated the phases inside SiO particles after the thermal annealing of a mixture of SiO and NaOH. The cross-section of Si-based multicomponents was obtained from a focused ion beam (FIB) that uses Ga ions to etch the samples‡. The cross-sectioned specimens were measured by transmission electron microscopy (TEM) in the dark-field mode, as shown in Fig. 2. The bright spots correspond to regions with higher electron density. As the amount of NaOH increased, the regions of bright spots became larger. Energy dispersive X-ray spectroscopy (EDAX) analysis from bright and dark regions of a representative sample (seen in Fig. 2c) confirmed that bright spots corresponded to the Si-rich regions, while dark spots indicated that the $x$ value of $SiO_x$ is close to 1 (Fig. 2d). From HR-TEM analysis, we confirmed that the Si-rich regions consisted of nano-crystalline Si (ESI, Fig. S6†). It should be noted that the amount of Si dispersed within the SiO matrix increased with the increasing NaOH contents, which was in good agreement with the XRD results seen in Fig. 1.

The solid SiO and Si–SiO–$SiO_2$ three-component electrodes were used as anode materials in LIBs. Since the Si-based materials have poor electrical conductivity, carbon layers were coated onto the surface of particles with carbon contents of 10 wt%, *via* thermal decomposition of acetylene gas at 900 °C for 10 min. The electrochemical performances were tested using 2016 coin-type half-cells with a metallic lithium counter-electrode. The voltage profiles of carbon-coated SiO (c-SiO), carbon-coated Si–SiO–$SiO_2$ three-components obtained by a mixture of SiO and NaOH (20 : 1, w/w) (c-Si-multi-20–1), c-Si-multi-10–1, and c-Si-multi-5–1 electrodes were obtained at a 0.1 C rate between 0.005 V and 2.0 V (Fig. 3a). The first discharge capacities are 2090, 1670, 1260, and 1015 mA h $g^{-1}$ for the electrodes of c-SiO, c-Si-multi-20–1, c-Si-multi-10–1, and c-Si-multi-5–1, respectively, with the corresponding coulombic efficiencies of 74.5, 78.0, 79.7, and 78.0%. The higher coulombic efficiencies of c-Si-multi-electrodes in the first cycles may be attributed to the cristobalite layer in the outer shells of the particles, which may act as a solid electrolyte interface (SEI) layer, as described in a previous report.[32]

Fig. 3b shows the differential capacity (d$Q$/d$V$) plots of c-SiO and c-Si-multi-20–1 electrodes during the first and second cycles. The irreversible reaction of c-SiO can be identified on the d$Q$/d$V$ plot. An intense peak at 0.25 V was seen in the first discharging, which was not observed from the second cycle. Kim *et al.* reported that the peaks seen at 0.25 V are caused by the formation of lithium silicate ($Li_4SiO_4$) and lithium oxide ($Li_2O$) in the first discharging of SiO using nuclear magnetic spectroscopy analysis.[33] The other peaks in the first and second cycles, which appeared at 0.23 and 0.08 V on discharging and at 0.28 and 0.45 V on charging (indicated by arrows in Fig. 3b), are assignable as a reversible reaction, similar to those of amorphous Si electrodes.[34] In contrast, the d$Q$/d$V$ plots of c-Si-multi-20–1 showed a very weak peak at 0.25 V, indicating small amounts of $Li_4SiO_4$ and $Li_2O$ products formed in the first discharge. It may result in the enhanced coulombic efficiency of the c-Si-multi-electrodes.

Fig. 3c shows the cycle performances of c-SiO (black), c-Si-multi-20–1 (red), c-Si-multi-10–1 (pink), and c-Si-multi-5–1 (blue) electrodes at the 0.1 C rate in the range of 0.005–2.0 V. Three c-Si-multi-electrodes showed excellent cycling retention of >99.5% after 100 cycles. As mentioned earlier, the thermally annealed SiO particles were converted to Si–SiO–$SiO_2$ three-component structures, in which

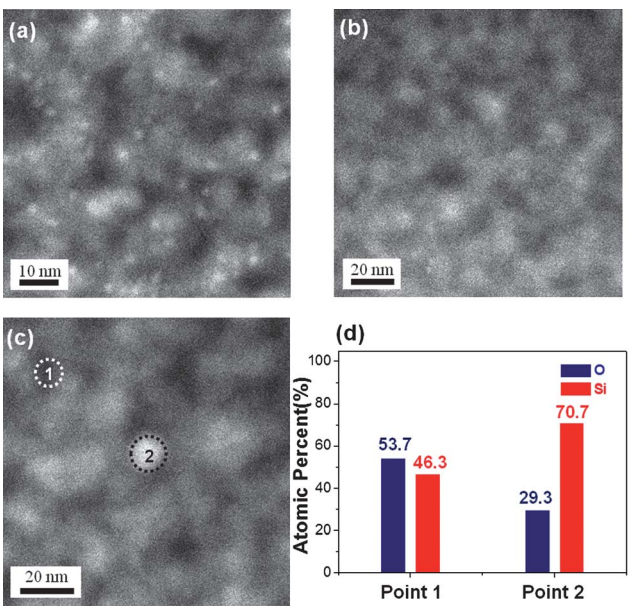


**Fig. 2** Dark-field TEM images of Si-based multicomponents. Three different samples were obtained by annealing at 800 °C as a function of NaOH amount (weight ratio of SiO to NaOH, (a) 20 : 1, (b) 10 : 1, and (c) 5 : 1), and the FIB cross-sections were measured by TEM. (d) From the sample seen in (c), two different spots (1 and 2) were analyzed by EDAX to investigate the atomic percent of Si and O.

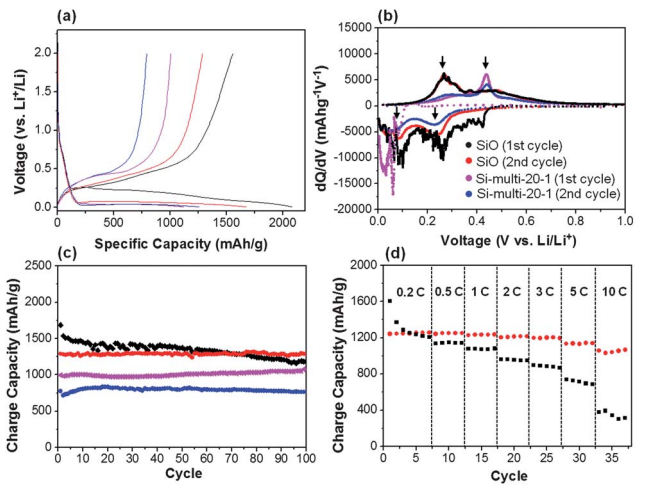


**Fig. 3** Electrochemical performances of c-SiO and c-Si–SiO–$SiO_2$ three-component electrodes. (a) Voltage profiles of c-SiO (black), c-Si-multi-20–1 (red), c-Si-multi-10–1 (pink), and c-Si-multi-5–1 (blue). (b) d$Q$/d$V$ plots of c-SiO and c-Si-multi-20–1 (red) in the first and second cycles. (c) Cycle performances of c-SiO (black), c-Si-multi-20–1 (red), c-Si-multi-10–1 (pink), and c-Si-multi-5–1 (blue) at 0.1 C rate. (d) Rate capabilities of c-SiO and c-Si-multi-20–1 electrodes. The discharge rate was fixed at a rate of 0.1 C.

nanocrystalline Si was uniformly dispersed within a SiO matrix and the crystalline silica formed on the outer surface. The nanocrystalline Si contributed to the high capacity, while $Li_2O$ formed in the first cycle and crystalline silica acted as a buffer layer to alleviate the large volume change of c-Si-multi-electrodes. This resulted in a highly stable cycle performance of the c-Si-multi-electrodes. Long-term cycling tests of c-Si-multi-20–1 at 0.1 C (120 cycles) and 0.2 C (80 cycles) showed Li extraction capacity retention of 99.5% after 200 cycles (ESI, Fig. S7†).

Moreover, the rate capabilities of the c-SiO and the c-Si-multi-20–1 were tested in the range from 0.1 C to 10 C rates. The c-SiO exhibited the poor capacity retention of 21% at 10 C, compared to that at 0.1 C, while the c-Si-multi-20–1 electrode showed a remarkable capacity retention of 84% at 10 C. This may be attributed to the minimization of the $Li_4SiO_4$ and $Li_2O$ amounts, which can prevent accessibility of lithium ions. In the case of the c-Si-multi-electrode, during the thermal annealing process, SiO was decomposed to Si, $SiO_2$, and remaining SiO. Therefore, the reduced amount of SiO may minimize the formation of $Li_2O$ and $Li_4SiO_4$, indicating the improvement of accessibility of lithium ions. Another piece of evidence for superior rate capability of the c-Si-multi-electrode is provided by the morphologies of silicon phase after 100 cycles. The TEM image of the c-Si multi-sample showed that the Si nanoparticles having an average diameter of 15 nm were randomly dispersed in the matrix consisting of $SiO_x$ and $Li_2O$, without a serious aggregation of nanoparticles, compared to that of the c-SiO electrode (ESI, Fig. S8†).

For the comparison study, we used a typical thermal decomposition process of SiO powders. When the SiO powder was heated at 1000 °C for 3 hr without NaOH, it disproportionated Si and amorphous $SiO_2$, as described in other reports.[22,28] The carbon-coated disproportionated SiO (d-SiO) showed a discharging capacity of 2074 mA h $g^{-1}$, with a coulombic efficiency of 75.4%. Also, the d-SiO electrode exhibited a capacity retention of 90% at the 0.1 C rate after 50 cycles. The electrochemical performances of the d-SiO are slightly better than those of carbon-coated SiO, but it did not exceed the performances of c-Si-multi-electrodes (ESI, Fig. S9†).

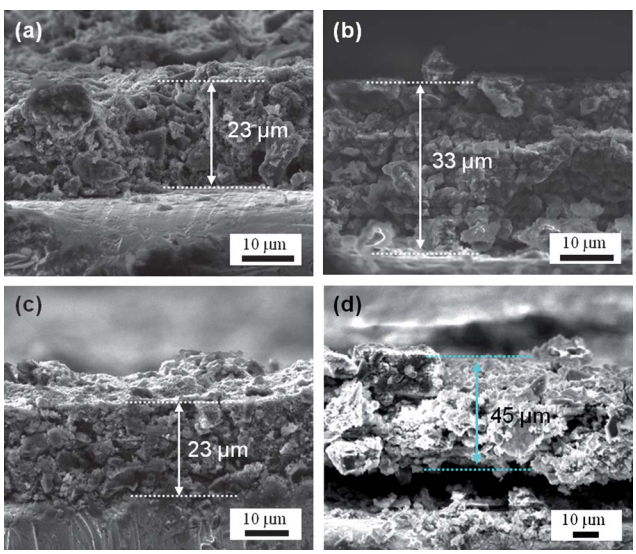


**Fig. 4** SEM images showing thickness of electrode materials before lithiation and after 200 cycles. Thickness of c-Si-multi-20–1 electrodes (a) before lithiation and (b) after 200 cycles at 0.2 C. Thickness of c-SiO electrodes (c) before lithiation and (d) after 200 cycles at 0.2 C. The Si-based multicomponent material showed less volume expansion than the SiO electrode.

**Table 1** Energy densities of c-SiO and c-Si-multi-20–1 electrodes

| Sample[a] | Before lithiation | After 200 cycles | Mass of active materials | Volume change | Energy density per volume |
|---|---|---|---|---|---|
| c-Si-multi | 23 μm | 33 μm | 6 mg | 49% | 1160 mA h $cm^{-3}$ |
| c-SiO | 23 μm | 45 μm | 6 mg | 90% | 830 mA h $cm^{-3}$ |

[a] Area of electrode: 2 $cm^2$.

Another advantage of the c-Si-multi-electrodes is a significantly reduced volume expansion after 200 cycles, resulting in an enhancement of the volumetric capacity (ESI, Fig. S9†). The c-SiO electrode expanded the volume to 90% after cycling, while the c-Si-multi-electrode showed less volume expansion (49%), as shown in Fig. 4. The volumetric energy density of the c-Si-multi-electrode was calculated to be ~1160 mA h $cm^{-3}$, compared to c-SiO (~830 mA h $cm^{-3}$), as summarized in Table 1. This may be attributed to the desirable structure of the electrode materials that are composed of a Si/SiO core and a $SiO_2$/carbon shell.

## Conclusions

We demonstrated a simple, but straightforward process for synthesizing Si–SiO–$SiO_2$ multicomponent particles from a commercially available solid SiO particle *via* a high-temperature annealing process in the presence of sodium hydroxide. The use of alkaline solution enabled us to lower the decomposition temperature of SiO. The carbon-coated Si–SiO–$SiO_2$ electrodes exhibited a remarkably improved electrochemical performance, including enhanced initial coulombic efficiency, highly stable cycling performance, a high reversible specific capacity, and increased volumetric energy density. It is strongly believed that our strategies will open up an avenue to synthesize high-performance anode materials for practical lithium-ion batteries.

## Acknowledgements

This work was supported by the MKE/ITRC program of NIPA (NIPA-2012-C1090-1200-0002) and the WCU (R31-2008-000-20012-0) programs.

## Notes and references

‡ Commercially available silicon monoxide (SiO, 325 mesh) was purchased from Aldrich. 10 g of SiO and 0.5–2 g of sodium hydroxide (NaOH) were mixed in 20 mL ethanol. After removing the ethanol completely, the mixture of SiO and NaOH was put into an alumina crucible and transferred to a quartz tube furnace. The furnace was heated to 800 °C at a rate of 5 °C $min^{-1}$ under an argon stream, and then held at this temperature for 10 min. Subsequently, it was cooled down to room temperature at a rate of 5 °C $min^{-1}$. During the thermal annealing process, the SiO was converted to Si–SiO–$SiO_2$ three-component (Si-based multicomponent) particles. The as-prepared samples were rinsed with de-ionized water to remove untreated NaOH, and followed by rinsing with 10% acetic acid to remove sodium silicate that formed during the chemical reaction of SiO and NaOH. Bare SiO and as-synthesized Si-based multicomponent particles were coated with a carbon layer (10 wt% carbon content) which was prepared *via* a thermal decomposition of acetylene gas at 900 °C for 10 min under an argon stream. The crystal

structures of SiO and Si-based multicomponent were measured by an X-ray diffractometer (XRD) on a Rigaku D/MAX at 2500 V using $Cu_{K\alpha}$ radiation. Raman spectra were recorded on a JASCO spectrometer (NRS 3000) to investigate the characteristics of carbon layers coated onto the surface of the SiO and the Si-based multicomponent. A He–Ne laser was operated at $\lambda = 632.8$ nm. To obtain the cross-sections of the Si-based multicomponent samples, a focused ion beam (Quanta 3D FEG) was operated using Ga-ions. A JEM-1400 (JEOL) transmission electron microscope (TEM), operating at an accelerating voltage of 200 kV, was used to observe the cross-section. The surfaces of Si-based multicomponent samples were characterized by a scanning electron microscope (NanoSEM 230, FEI) operating at 10 kV with a 3 nm thick Pt coating layer. The electrochemical test was performed using coin-type half-cells (2016 R-type) assembled in an argon-filled glove box. Carbon-coated SiO and Si-based multicomponent powders as the working electrode and lithium metal as the counter-electrode were used. The electrode for the cell test was made of an Si-based active material (60 wt%), Super P carbon black (20 wt%), and poly(acrylic acid)/sodium carboxymethyl cellulose (50 : 50, w/w) binder (20 wt%). The electrolyte was $LiPF_6$ (1.3 M) with ethylene carbonate/diethylene carbonate (EC/DEC, 30 : 70 vol%, Panax Starlyte, Korea). The coin-type half-cells were cycled at a rate of 0.1–10 C between 0.005 and 2.0 V.


1 M. Armand and J.-M. Tarascon, *Nature*, 2008, **451**, 652.
2 A. Manthiram, A. V. Murugan, A. Sarkar and T. Muraliganth, *Energy Environ. Sci.*, 2008, **1**, 621.
3 M.-K. Song, S. Park, F. M. Alamgir, J. Cho and M. Liu, *Mater. Sci. Eng., R*, 2011, **72**, 203.
4 C. K. Chan, H. Peng, G. Liu, K. McIlwrath, X. F. Zhang, R. A. Huggins and Y. Cui, *Nat. Nanotechnol.*, 2008, **3**, 31.
5 C. Liu, F. Li, L.-P. Ma and H.-M. Cheng, *Adv. Mater.*, 2010, **22**, E28.
6 C. K. Chan, X. F. Zhang and Y. Cui, *Nano Lett.*, 2008, **8**, 307.
7 H. Kim and J. Cho, *Chem. Mater.*, 2008, **20**, 1679.
8 P. L. Taberna, S. Mitra, P. Poizot, P. Simon and J.-M. Tarascon, *Nat. Mater.*, 2006, **5**, 567.
9 P. Poizot, S. Laruelle, S. Grugeon, L. Dupont and J.-M. Tarascon, *Nature*, 2000, **407**, 496.
10 U. Kasavajjula, C. Wang and A. J. Appleby, *J. Power Sources*, 2007, **163**, 1003.
11 A. Magasinski, P. Dixon, B. Herzberg, A. Kvit, J. Ayala and G. Yushin, *Nat. Mater.*, 2010, **9**, 353.
12 M.-H. Park, M. G. Kim, J. Joo, K. Kim, J. Kim, S. Ahn, Y. Cui and J. Cho, *Nano Lett.*, 2009, **9**, 3844.
13 J. Saint, M. Morcrette, D. Larcher, L. Laffont, S. Beattie, J. P. Peres, D. Talaga, M. Couzi and J.-M. Tarascon, *Adv. Funct. Mater.*, 2007, **17**, 1765.
14 Y. S. Hu, R. Demir-Cakan, M. M. Titirici, J. O. Muller, R. Schlogl, M. Antonietti and J. Maier, *Angew. Chem., Int. Ed.*, 2008, **47**, 1645.
15 G. Derrien, J. Hassoun, S. Panero and B. Scrosati, *Adv. Mater.*, 2007, **19**, 2336.
16 Y. Zhang, X. G. Zhang, H. L. Zhang, Z. G. Zhao, F. Li, C. Liu and H. M. Cheng, *Electrochim. Acta*, 2006, **51**, 4994.
17 J. Chen, A. I. Minett, Y. Liu, C. Lynam, P. Sherrell, C. Wang and G. G. Wallace, *Adv. Mater.*, 2008, **20**, 566.
18 M. N. Obrovac and L. J. Krause, *J. Electrochem. Soc.*, 2007, **154**, A103.
19 H. L. Zhang, F. Li, C. Liu and H. M. Cheng, *J. Phys. Chem. C*, 2008, **112**, 7767.
20 T. Morita and N. Takami, *J. Electrochem. Soc.*, 2006, **153**, A425.
21 C.-H. Doh, H.-M. Shin, D.-H. Kim, Y.-C. Ha, B.-S. Jin, H.-S. Kim, S.-I. Moon and A. Veluchamy, *Electrochem. Commun.*, 2008, **10**, 233.
22 C.-M. Park, W. Choi, Y. Hwa, J.-H. Kim, G. Jeong and H.-J. Sohn, *J. Mater. Chem.*, 2010, **20**, 4854.
23 H. Nara, T. Yokoshima, T. Momma and T. Osaka, *Energy Environ. Sci.*, 2012, **5**, 6500.
24 G. W. Brady, *J. Phys. Chem.*, 1959, **63**, 1119.
25 H. R. Philipp, *J. Non-Cryst. Solids*, 1972, **8–10**, 627.
26 E. Füglein and U. Schubert, *Chem. Mater.*, 1999, **11**, 865.
27 A. Hohl, T. Wieder, P. A. van Aken, T. E. Weirich, G. Denninger, M. Vidal, S. Oswald, C. Deneke, J. Mayer and H. Fuess, *J. Non-Cryst. Solids*, 2003, **320**, 255.
28 M. Mamiya, M. Kikuchi and H. Takei, *J. Cryst. Growth*, 2002, **237**, 1909.
29 B. D. Cullity, *Elements of X-Ray Diffraction*, Addison-Wesley, Massachusetts, 1978.
30 W. S. Fyfe and S. McKay, *Am. Mineral.*, 1962, **47**, 83.
31 P. Bettermann and F. Liebau, *Contrib. Mineral. Petrol.*, 1975, **53**, 25.
32 T. Zhang, J. Gao, H. P. Zhang, L. C. Yang, Y. P. Wu and H. Q. Wu, *Electrochem. Commun.*, 2007, **9**, 886.
33 T. Kim, S. Park and S. M. Oh, *J. Electrochem. Soc.*, 2007, **154**, A1112.
34 M. N. Obrovac and L. Christensen, *Electrochem. Solid-State Lett.*, 2004, **7**, A93.